nature communications

Article

https://doi.org/10.1038/s41467-025-64151-1

# Enantioselective homologation of helical architectures from fluorenones to phenanthrenones with enhanced circular dichroism

Received: 9 May 2025

Accepted: 8 September 2025

Published online: 13 October 2025

Check for updates

Shiyang Li, Shi Yan, Zhenzhong Liu, Yang Zhang, Yuqiao Zhou, Xiaoming Feng, Liang-Wen Feng ✉ & Xiaohua Liu ✉

The development of efficient synthetic methods to access optically pure helical chiral molecules is a central challenge in organic chemistry due to their unique photophysical properties and potential applications in chiral photonic devices. Conventional strategies often struggle to simultaneously install multiple chiral elements with high fidelity and are typically limited to synthesizing a single scaffold at a time. Here we show that a chiral Sc(III)-catalyzed ring-expansion of racemic helical fluorenones with α-diazo esters, enables the simultaneous synthesis of both optically enriched helical fluorenones and one-carbon-inserted helical phenanthrenones with high diastereo- and enantioselectivity. This process achieves simultaneous kinetic resolution and homologation, but also intriguing regioselectivity at the cases of un-symmetric ketones. Furthermore, the synthesized helical compounds exhibit significant chiroptical activity, with their circularly polarized absorption dissymmetry factors ($g_{abs}$) showing a strong dependence on the position and steric nature of aryl substituents, and some derivatives also display circularly polarized luminescence (CPL).

Helicenes and helicenoids are a class of helical molecules in which steric repulsion between terminal aromatic rings induces a twisted, helical framework[1]. This distortion of the π-conjugated system confers unique chiroptical and electrical properties, such as optical rotation, electronic circular dichroism (CD), and circularly polarized luminescence (CPL)[2–5]. Due to these distinctive features, the precise synthesis of enantiomerically enriched helicenes with diverse architectures has attracted considerable interest in material science, and chiral catalysis[6–11]. Compared to the flourishing progress in central chirality construction, synthetic strategies for helical chirality remain relatively limited. Among the available synthetic strategies, transition metal catalyzed asymmetric transformations, including [2 + 2 + 2] cycloisomerization, hydroarylation, olefin metathesis and biaryl coupling, have significantly advanced the construction of chiral helicenes and helicenoids[12–39]. For example, in 2009, Tanaka and coworkers utilized a rhodium(I)/chiral bis-phosphine-catalyzed asymmetric intermolecular double [2 + 2 + 2] cycloisomerization to assemble a [9] helical fluorenone framework, albeit with moderate yield and enantioselectivity[40]. Later, this approach enabled efficient construction of [7]helical fluorenones (Fig. 1A)[41]. Alternatively, the Oestreich's group attempted to construct [7]helical fluorenones via a palladium-catalyzed carbonylative reaction of optically pure axially chiral biaryls (Fig. 1B)[42]. However the axial chiraltiy transferred to helical chirality did not work well as a result of racemization at high reaction temperature. The design of innovative and general enantioselective synthetic routes to access new families of chiral substituted helical

Key Laboratory of Green Chemistry & Technology, Ministry of Education, College of Chemistry, Sichuan University, Chengdu, China.
✉e-mail: liangwenfeng@scu.edu.cn; liuxh@scu.edu.cn

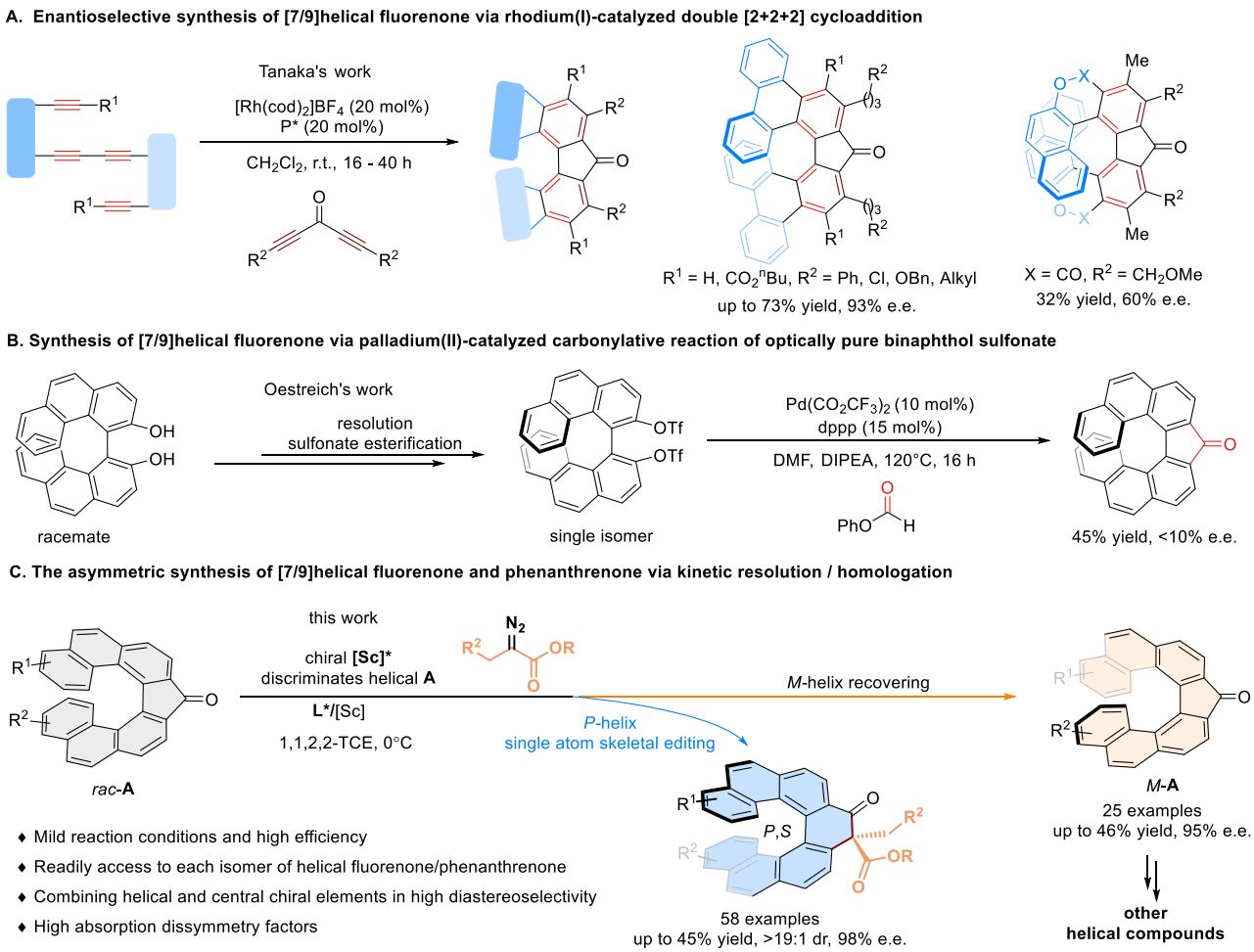


**Fig. 1 | Background information about asymmetric synthesis of helical fluorenones. A** Rhodium(I)-catalyzed enantioselective intermolecular double [2 + 2 + 2] cycloaddition. **B** Palladium(II)-catalyzed carbonylative reaction using optically pure binaphthol sulfonate as the starting materials. **C** Kinetic resolution of helical fluorenones and synthesis of helical phenanthrenones via enantioselective homologation.

fluorenones and their structurally diverse derivatives remains a significant and ongoing challenge.

The kinetic resolution strategy offers a complementary approach to simultaneously access enantiomerically pure starting materials and their derivatives. Moreover, carbonyl homologation using α-diazo compounds[43,44] represents a powerful tool for precision single-atom skeletal editing in organic synthesis. We envisioned that integrating this homologation process into the kinetic resolution of helical fluorenones could concurrently enable the construction of structurally diverse helical phenanthrenones (Fig. 1C). Building on our prior work in enantioselective carbonyl homologation and others[45–54], we identified several key challenges in adapting this transformation to helical fluorenones: (1) Catalyst design: a stronge Lewis acid catalyst paired with a tailored chiral ligand is essential to promote ketone homologation, leveraging ligand-accelerated catayasis[55]. (2) Enantiomer discrimiantion: effective resolution requires precise discrimination of the two up-and-down terminal aromatic rings distal to the metal center. (3) Stereoselectivity: the helical phenanthrenone product incorporate both helical and central chiralities, complicating diastereo- and enantiocontrol due to the symmetric, unbiased ketone substitution pattern. In addition, the reaction become further challenging with regioselectivty for un-symmetric ketones. Herein, we report a mild and efficient enantioselective homologation of racemic helical fluorenones by a chiral scandium(III) complex (Fig. 1C). Unlike traditional resolution methods, this strategy eliminates the need for chiral auxiliaries or chromatographic separation. A broad range of optically pure symmetric and unsymmetric [6/7]helical fluorenones and their ring-expanded [5/6/7]helical phenanthrenones, as well as other modified helical compounds were synthesized in high yield and high optical activity. Through stereodivergent synthesis, we accessed both enantiomers of [7]helical fluorenone and all four stereoisomers of [7]helical phenanthrenone. These compounds enable systemically investigation of photophysical and chiroptical properties, revealing strong correlation between structures and $|g_{abs}|$ values.

## Results

### Investigation of reaction conditions

Our study began with an evaluation of the kinetic resolution/skeletal editing of [7]helical fluorenone **A1** with methyl α-diazo ester **B1'** by the use of various chiral scandium(III) catalysts (for details see Supplementary Information Table S1–8). The homologation reaction was highly dependent on the catalyst components, occurring only in the presence of particular *N,N'*-dioxide ligands and with $Sc(OTf)_3$ as the metal precursor. For ligand skeletons, *L*-pipecolic acid derived ones were favorable in terms of reactivity and enantioselectivity, beating other amino acid derived analogues (for details see Supplementary Information Table S2). As shown in Table 1, when *L*-pipecolic acid-based *N,N'*-dioxides were evaluated, it was found that the reactivity is also sensitive to the ligand structures with variation at amide substitutions. Ligand **$L_3$-PiPr$_2$** containing steric hindered 2,6-diisopropyl aniline substituents hampered the reaction, leading to no homologation reaction and resolution (Table 1, entry 3 vs entries 1 and 2). Thus,

https://doi.org/10.1038/s41467-025-64151-1

## Table 1 | Reaction development and standard conditions

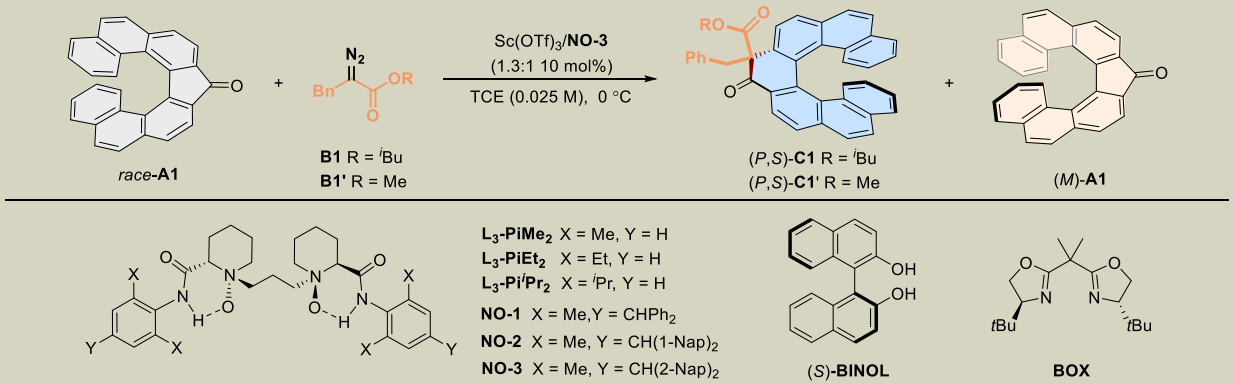


| Entry[a] | Condition variation | C | | A1 | | |
|---|---|---|---|---|---|---|
| | | Yield (%)[b] | d.r.[b] | e.e. (%)[c] | Yield (%)[b] | e.e. (%)[c] |
| 1 | **$L_3$-PiMe$_2$, B1'**, 35 °C, DCM (0.05 M) | 31 (**C1'**) | 4.8:1 | 80/76 | 69 | 22 |
| 2 | **$L_3$-PiEt$_2$, B1'**, 35 °C, DCM (0.05 M) | 45 (**C1'**) | 3.6:1 | 77/66 | 55 | 35 |
| 3 | **$L_3$-Pi$^i$Pr$_2$, B1'**,35 °C, DCM (0.05 M) | N.R. | - | - | 100 | 0 |
| 4 | **NO-1, B1'**, 35 °C, DCM (0.05 M) | 20 (**C1'**) | 5.0:1 | 80/73 | 80 | 15 |
| 5 | **NO-2, B1'**, 35 °C, DCM (0.05 M) | 27 (**C1'**) | 6.8:1 | 83/45 | 83 | 24 |
| 6 | **NO-3, B1'**, 35 °C, DCM (0.05 M) | 31 (**C1'**) | 7.0:1 | 91/70 | 69 | 32 |
| 7[d] | **NO-3, B1'**, 35 °C, DCM (0.025 M) | 48 (**C1'**) | 5.3:1 | 90/80 | 52 | 57 |
| 8[d] | **NO-3, B1**, 35 °C, DCM (0.025 M) | 57 (**C1**) | 5.2:1 | 95/91 | 43 | 87 |
| 9[d] | **NO-3, B1**, DCM (0.025 M) | 29 (**C1**) | 12.0:1 | 95/91 | 71 | 33 |
| 10[d] | **NO-3, B1**, TCE (0.025 M) | 49 (**C1**) | 8.7:1 | 98/93 | 51 | 80 |
| 11[d,e] | **NO-3, B1**, TCE (0.025 M), 8 h | 55 (**C1**) | 7.8:1 | 98/93 | 45 | 94 |
| 12[d,e] | **NO-3, B1**, TCE (0.025 M), 6 h | 51 (**C1**) | 8.3:1 | 98/91 | 49 | 82 |
| 13[d,e] | **BINOL** or **BOX, B1**, TCE (0.025 M) | N.R. | - | - | 100 | 0 |

[a]Unless otherwise noted, the reactions were carried out with **A1** (0.05 mmol), diazo ester **B** (0.025 mmol), Sc(OTf)$_3$/**L*** (1.3:1, 10 mol%) in solvent under air atmosphere for 12 h.
[b]Determined by $^1$H NMR, 0.05 mmol 1,1,2,2-tetrachloroethane was added as an internal standard.
[c]Determined by UPCC and HPLC.
[d]With diazo ester **B** (1.25 equiv.).
[e]Sc(OTf)$_3$/**L*** was activated in THF for 30 min at 35 °C, then THF was evaporated.

consequent ligand modification focused on introducing substitution at the *para*-position of 2,6-dimethylaniline to expand the chiral pocket for discrimination of terminal aryls (Table 1, entries 4-6). Installing *para*-diphenylmethanyl substituents (ligand **NO-1**) exhibited minimal impact on the reaction performance. Notably, the introduction of conjugate naphthyl groups significantly altered the enantioselectivity and diastereoselectivity of the kinetic resolution/skeletal editing process (Table 1, entries 5 and 6). When employing ligand **NO-3**, the [7]helical phenanthrenone derivative **C1'** was isolated in 31% yield with enantioselectivity being enhanced to 91% ee of the major diastereomer (7.0:1 dr), while the starting material **A1** was recovered in 32% e.e. (Table 1, entry 6).

Through reduce of reaction concentration and adjust the substrates ratio (Table 1, entry 7), the conversion increased to 48% along with slightly higher ee value for helical fluorenone **A1** (57% e.e.). Next, we examined the influence of the ester group of α-diazo compounds to further improve the results (for more details see Supplementary Information Table S7). When *iso*-butyl diazoester **B1** was used, the corresponding [7]helical phenanthrenone derivative **C1** was isolated in 57% yield, 5.2:1 dr and up to 95% e.e., meanwhile the helical fluorenone **A1** was recovered in 43% yield and 87% e.e. (Table 1, entry 8). Decreased reaction temperature was beneficial to diastereoselectivity but the conversion was reduced (Table 1, entry 9). Through systematic investigation of solvents and temperature (for details see Supplementary Information Tables S4 and S6), we ultimately discovered that employing 1,1,2,2-TCE as solvent at 0 °C significantly improved the ee value of the product **C1** to 98% without compromising conversion efficiency, while enabling 51% recovery of helical fluorenone **A1** with 80% e.e. (Table 1 entry 10). To solve the poor solubility of $Sc(OTf)_3$ in 1,1,2,2-TCE, THF was employed as prosolvent for chiral catalyst preparation. This pre-treatment significantly enhanced the catalytic activity (Table 1, entries 11 and 12). Ultimately, kinetic resolution through homologation after controlled reaction time gave raise to two kinds of helical chiral compounds in considerable yield and excellent enantioselectivity (entry 11; **C1**/98% e.e., and **A1**/94% e.e.). Following the similar procedure using other chiral ligands, such as BINOL and BOX, no desired transformation occurred (Table 1, entry 13), manifesting obvious ligand acceleration[55].

## Substrates scope of helical fluorenones

With the optimized reaction conditions in hand, the substrate scope of helical fluorenones was evaluated (Fig. 2). A series of optically enriched [7]helical phenanthrenone derivatives (**C2**–**C17**) and substituted [7]helical fluorenones (**A2**–**A17**) were available through homologation-involved kinetic resolution. On the whole, the position of substituents on the aryl ring of [7]helical fluorenones exhibited minimal influence on the outcome of the reaction, except for those with substituents at the 4,4'-position (**A4, A9** and **A16**). For these three cases, it is not easy to leverage the stereoselectivity and yield, and these products were obtained in high diastereo- and enantioselectivity at the cost of conversion or optical activity of the recovered substrates. The homologation activity is closely related to the electronic effect of the substituents. Substrates (**A2**–**A6, A10** and **A12**–**A14**) with electron-donating alkyl groups, regardless positions and steric hindrance, exhibited higher reactivity, requiring shorter reaction times (4–5 h) than helical fluorenones (**A7**–**A9, A11** and **A17**) with electron-withdrawing aryl groups (8–12 h). These reactions delivered the desired [7]helical phenanthrenone derivatives (**C2**–**C17**) in 42–50% yield, 4.9:1 to 13.7:1 dr and 91–99% e.e. for all diastereomers. The corresponding [7]helical fluorenones could be recovered in 38–47% yield with 80–97% e.e. Racemic phenyl-substituted **A15** underwent the reaction in a stereoselective manner to yield **C15** in 45% yield, 11.2:1 d.r. and 97% ee after a longer time, and kinetic resolution lead to enantiomerically enrich **A15** (90% e.e.) in 45% yield. Heterocycle-bearing [7]helical fluorenones, such as thiophene-fused **A18** and furan-fused **A19** exhibit higher reactivity and resolution efficiency within 3 h, but the excellent results maintained even after 24 h. The process could also be applied to naphthalene-fused [9]helical fluorenone **A20** although its behavior was similar to 4,4'-substituted ones. The related [9]helical phenanthrenone **C20** was isolated in 41% yield, 8.4:1 d.r. with 97% e.e., accompanied by recovering **A20** in 49% yield with 77% e.e.

Through X-ray crystallographic analysis, the recovered [7]helical fluorenone **A18** was determined to be *M*-configuration (Fig. 2). The other recovered helical fluorenones were also assigned as the same configuration based on circular dichroism (CD) spectroscopy analysis. Oppositely, the *P*-configured isomers prefer to perform the ring-expansion under the catalysis. The relative configuration of the major diastereomer of the racemic [7]helical phenanthrenone **C6** is assigned as *rel*-(*P*, *S*) or *rel*-(*M*, *R*) based on X-ray crystallographic analysis. Accordingly, the absolute configuration of asymmetric catalytic product **C6** was assigned as (*P*, *S*). The configuration of the other major isomers of helical phenanthrenones following the same arrangement from the corresponding CD spectroscopy.

The catalytic system also enables efficient kinetic resolution of unsymmetric [6/7]helical fluorenones (Fig. 3), manifesting good regio-, diastereo-, and enantioselectivity. Similarly, (*M*)-fluoreones (**A21**–**A25**) were recovered as the less reactive isomers (36–54% yields, 67–98% e.e.). (*P*)-fluoreones (**A21**–**A25**) participated in homologation to give the ring-expanded [6/7]helical phenanthrenones (**C21**–**C25**) in which small substituent ($Ar^2$) shifted to generate the quaternary carbon center with good yields and ee values (43–50% yields, 93–95% e.e.). In comparison, (*P*)-[6]helical fluorenones (**A21**–**A23**) demonstrated high reactivity to achieve good yields within 3 h, accompanied by around 5% yield of isomers (**C21'**–**C23'**). The [6]helical fluorenone **A24** and [7]helical fluorenone **A25** exhibited diminished reactivity and longer reaction time was required. And the former one suffered ring-expansion of (*M*)-isomer to yield (*M*, *S*)-**C24'** in 14% isolated yield and 96% e.e., which generated from the migration of fused-aryl group based on X-ray crystal analysis. The arrangement of the major product **C25** was assigned as (*P*, *S*) concluded from the X-ray crystal of the related racemate as well as CD spectra. In addition, [5]helicene fluorenones **A26** and **A27** underwent complete conversion, affording the ring-expanded product **C26** with high enantioselectivity and diastereoselectivity (89% yield, 18/1 d.r., 93% e.e.) at 35 °C, and two diastereomers of **C27** (1.3:1 d.r.) with comparable high enantioselectivity at 35 °C, respectively (for details see Supplementary Information Table S9).

## Substrates scope of α-Diazo esters

To further explore the substitution variety of [7]helical phenanthrenones, a number of α-diazo esters with different substituents were tested (Fig. 4). It was obvious that α-diazo esters bearing electron-donating substituted benzyl groups participated in the reaction to get satisfied yield within shorter reaction time (less than 5 h), in comparison with these bearing electron-withdrawing groups (9–54 h). Substitutions at *meta*- and *para*-positions were all tolerable well, and different substituted [7]helical phenanthrenones (**D1**–**D25**) could be isolated in excellent enantioselectivity (95–99% e.e.). The *para*-methoxy substituted ones were more reactivity, and over-conversion resulted in reduced d.r. value (**D8, D21** and **D25**) and higher yield even within short reaction time, however, the diastereoselectivity of the others could achieve 6.0:1 to 15:1 at 40–50% yield. Noteworthily, 3-nitro-substitued **D18** could be obtained in 40% yield after longer reaction time. For cyanide and nitro-substituted ones (**D13, D17**, and **D18**), the reactivity drastically decreased, minimizing further occurrence of homologation even after prolonged reaction times. Both 2-naphthyl and 1-naphthyl substituted α-diazo esters could be edited into the helical structures (**D26** and **D27**), but the latter one required longer reaction time to achieve acceptable yield, with extremely high

https://doi.org/10.1038/s41467-025-64151-1

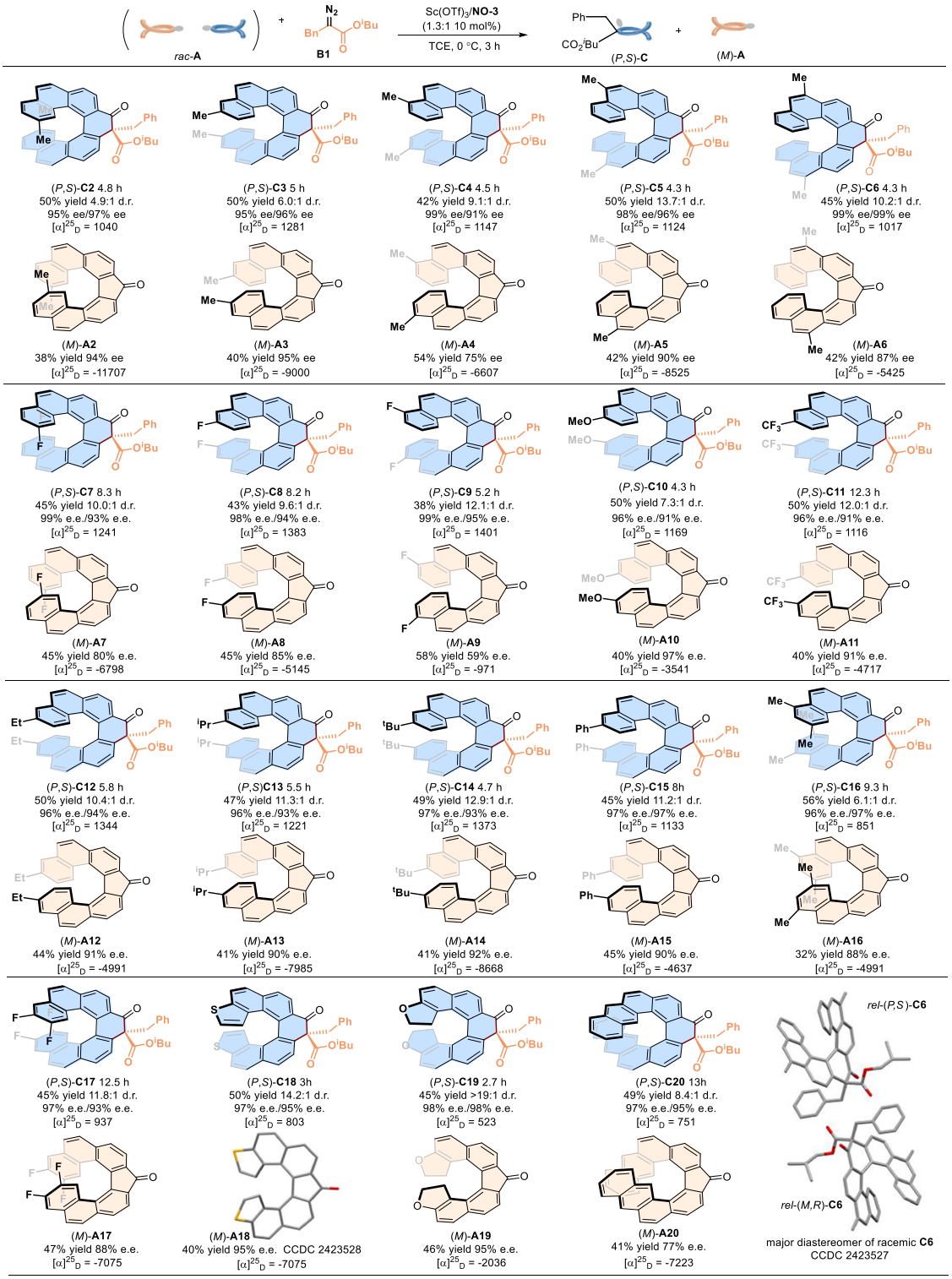


**Fig. 2 | Substrate scope of helical fluorenones.** All reactions were carried out with helical fluorenone **A** (0.05 mmol), diazo ester **B1** (1.25 equiv.), $Sc(OTf)_3$/**NO-3** (1.3:1, 10 mol%) in 1,1,2,2-TCE (0.025 M) under air atmosphere. Isolated yields after column chromatography separation. The d.r. value was determined by $^1H$ NMR spectroscopy and the e.e. value was determined by HPLC.

diastereo- and enantioselectivity (up to 19:1 d.r., and 98–99% e.e.). The benzofuran-containing **D28** and cinnamyl-containing **D30** were isolated in excellent results. In addition, indole and pyridine-substituted α-diazoesters were also tested, unfortunately, there is lack of analytical methods to determine the stereoselectivity of the products. In these reactions, the unreacted [7]helical fluorenone **A1** could be isolated in 35–52% yields, meanwhile the enantioselectivity dropped along with higher recover yield, confirming a kinetic resolution process. Alkyl-substituted diazo esters, such as phenethyl and stearyl derivatives, indeed exhibited attenuated reactivity. Under standard catalyst after 24 h, these substrates afford the products (**D31** and **D32**) in moderate yields with good enantioselectivity. In contrast, diazoesters bearing allyl, alkenyl, hydrogen, or phenyl substituents (**C33**–**C36**) demonstrate markedly diminished reactivity.

https://doi.org/10.1038/s41467-025-64151-1

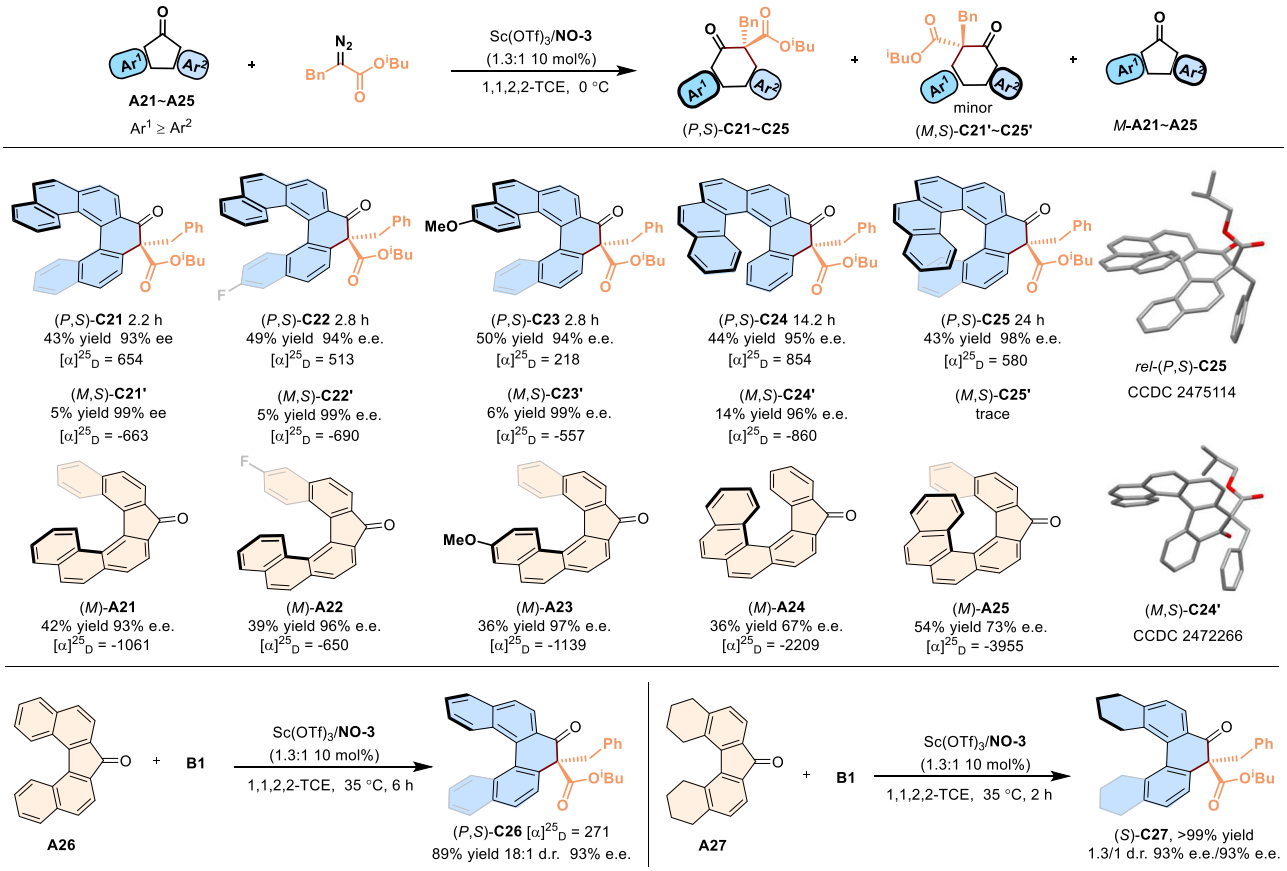


**Fig. 3 | Substrate scope of unsymmetric helical ketones and others.** Unless otherwise noted, the reaction condition is as same as in Fig. 2.

## Stereodivergent synthesis and synthetic applications

The potential of this method for the skeletal editing-based kinetic resolution of [7]helical fluorenones was further demonstrated by gram-scale synthesis. As shown in Fig. 5A, the stereodivergent synthesis was carried out with racemic [7]helical fluorenone **A1** (5.0 mmol) and α-diazo ester **B1** (6.25 mmol) under the standard reaction conditions catalyzed by Sc(III)/**NO-3** or Sc(III)/*ent*-**NO-3**. Thus, the [7]helical phenanthrenone product (*P, S*)-**C1** or (*M, R*)-**C1** could be isolated in comparable yield and stereoselectivity, at the same time, [7]helical fluorenone (*M*)-**A1** or (*P*)-**A1** could be obtained separately. Scale-up reaction performed well under the standard condition, and even reduced reaction time (3 h) was tolerable. As shown in Figs. 2 and 3, in all cases, the minor diastereomers could also be isolated in excellent enantioselectivity, manifested that chiral quaternary centers could be well controlled by the catalyst, which give chance for stereodivergent synthesis. If the isolated optically active *M*-**A1** and *P*-**A1** were resubjected into the original catalytic systems, after full transformations, the corresponding (*S, M*)-**C1** and (*R, P*)-**C1** could be isolated in up to >19/1 d.r. with 97% ee. Therefore, stereodivergent synthesis of the four isomers of [7]helical phenanthrenone bearing central and helical chirality could be readily achieved.

The synthetic transformations of the [7]helical fluorenone *M*-**A1** enabled the preparation of a series of [7]helical compounds (Fig. 5B). Reduction with $NaBH_4$ gave raise to (*M*)-[7]helical fluorenol **E1** in nearly quantitative yield. Both methyl and phenyl substituted [7]helical fluorenol (*M*)-**E2** and (*M*)-**E3** could be isolated in good yield after the treatment with Grignard reagents. The former **E2** has been used for synthesis of helically chiral carbenium ion, acting as carbon Lewis acid catalyst[42]. When using $Et_3SiH/BF_3{\cdot}OEt_2$ reducing system, the carbonyl group was directly reduced to a methylene group, delivering (*M*)-[7]helical fluorene **E4** in 78% yield, accompanied by un-identified by-products. The corresponding *O*-methyloxime (*M*)-**E5** and hydrazone (*M*)-**E6** could be quantitatively isolated after mixing helical fluorenone with $NH_2OMe{\cdot}$or hydrazine hydrate in pyridine. The hydrazone (*M*)-**E6** could be further converted to a diazo-containing helical compound (*M*)-**E7** using manganese dioxide as the oxidant and magnesium sulfate as a dehydrating agent. [7]Helical fluorene fused spiro cyclic derivative (*M*)-**E8** could be obtained from the coupling with 1-bromo-2-benzobenzene. By employing $BF_3{\cdot}OEt_2$ as the catalyst, skeletal editing of (*M*)-**A1** with $TMSCHN_2$ led to efficient synthesis of [7]helicene (*M*)-**E9** after acylation with isopropyl chloroformate. Moreover, upon undergoing straightforward decarbonylation followed by acylation protection, the ring-expanded product (*P, S*)-**D29** can be converted to the all-carbon-conjugated [7]helicene derivative (*P*)-**E10** in good yield. In all these transformations, the helical chirality could be maintained.

## Photophysical chiroptical properties

As illustrated in Fig. 6A, [7]helical fluorenone (*M*)-**A1** and its enantiomer (*P*)-**A1** display a mirror image of the spectral shapes of circular dichroism in dichloromethane. The robust Cotton effect in the high-energy band from 280 to 370 nm can be partly attributed to a mixture of n→π* and π → π* transition. There is weak and broad Cotton effect appeared in the low-energy band from 420 to 520 nm. The enantiomeric pair of [7]helical phenanthrenone (*P, S*)-**C1** and (*M, R*)-**C1** also exhibited mirror-symmetric CD spectra, and the diastereomer (*P, R*)-**C1** and (*P, S*)-**C1** had similar Cotton effect at 350 nm. The ring-expanded phenanthrenones showed blue shift of the absorption compared with fluorenone in the high-energy band, and the Cotton effect in the low-energy band disappeared. The dissymmetry factors ($g_{abs}$), calculated with the relationship $g_{abs} = \Delta\varepsilon/\varepsilon$, revealed distinct wavelength-dependent profiles. The maximum $|g_{abs}|$ of [7]helical fluorenone *M*-**A1** and [7]helical phenanthrenone (*P, S*)-**C1** reached $-7.7 \times 10^{-3}$ (at

https://doi.org/10.1038/s41467-025-64151-1

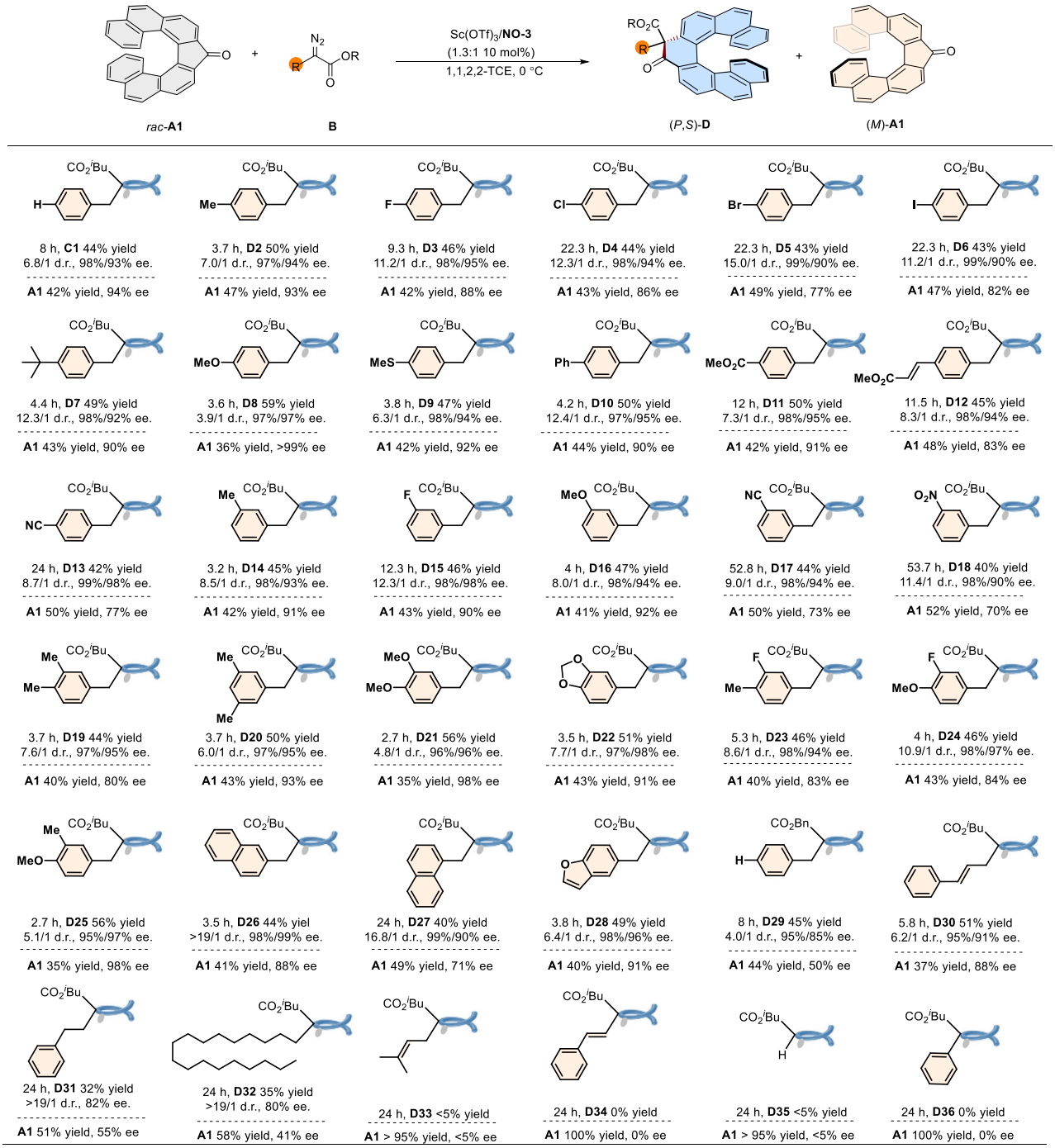


**Fig. 4 | Substrate scope of α-diazo esters.** Unless otherwise noted, the reactions were carried out with helical fluorenone **A1** (0.05 mmol), diazo compound **B** (1.25 equiv.), Sc(OTf)$_3$/**NO-3** (1.3:1, 10 mol%) in 1,1,2,2-TCE (0.025 M) under air atmosphere. Isolated yields after column chromatography separation. The d.r. value was determined by $^1$H NMR spectroscopy and the e.e. was determined by HPLC.

362 nm) and $+1.4 \times 10^{-2}$ (at 349 nm), respectively. The ring expansion and introduction of a chiral quaternary carbon center nearly doubled the asymmetric absorption factor compared to the [7]helical fluorenone **A1**.

To elucidate the origin of the enhanced $|g_{abs}|$ values, time-dependent density functional theory (TD-DFT) calculations were conducted at the PBE0/def2-TZVP level[56–59]. For each enantiomer of **A1**, the transition corresponding to the largest $|g_{abs}|$ was identified as $\mathbf{S_0} \rightarrow \mathbf{S_5}$ transition, whereas for each pair of enantiomers of **C1**, the dominant transition shifted to $\mathbf{S_0} \rightarrow \mathbf{S_4}$ transition. Theoretical analysis defines the dissymmetry factor of small organic molecules is usually simplified as $g_{abs} \approx 4\cos\boldsymbol{\theta}\,|\,\mathbf{m}\,|/|\,\boldsymbol{\mu}\,|$. The $g_{abs}$ value exhibits a correlation with both the $|\mathbf{m}|/|\boldsymbol{\mu}|$ ratio and the angle $\boldsymbol{\theta}$ between $\mathbf{m}$ and $\boldsymbol{\mu}$, where $\mathbf{m}$ and $\boldsymbol{\mu}$ represent the magnetic and electric transition dipole moments, respectively. Computational analysis of the [7]helical fluorenone **A1** and [7]helical phenanthrenone **C1** quantified these parameters which were shown in Fig. 6C. The enhancement in $|g_{abs}|$ stems from two key factors: a higher $|\mathbf{m}|/|\boldsymbol{\mu}|$ ratio in [7]helical phenanthrenone **C1** system compared to [7]helical fluorenone **A1** as well as decreased $\boldsymbol{\theta}$, leading to stronger alignment of $\boldsymbol{\mu}$ and $\mathbf{m}$ (Fig. 6D). These computational results align closely with experimental $g_{abs}$ measurements, confirming that structural modifications amplify chiroptical responses by

https://doi.org/10.1038/s41467-025-64151-1

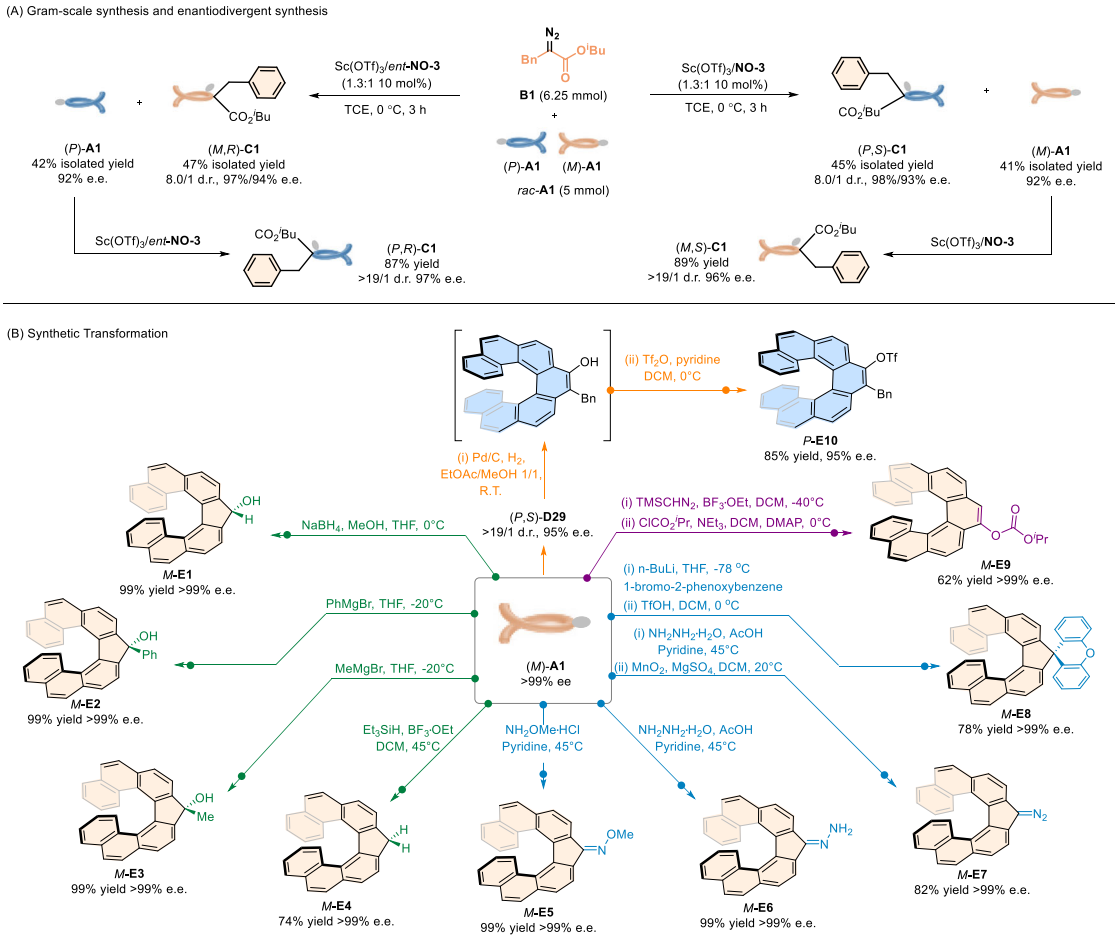


**Fig. 5 | Gram-scale synthesis, stereodivergent synthesis and synthetic applications. A** Gram-scale synthesis and stereodivergent synthesis all stereoisomers of **A1** and **C1**. **B** Further transformations of the (*M*)-**A1** and (*P,S*)-**C29**. Isolated yields after column chromatography separation.

synergistically enhancing magnetic transition contributions and dipole alignment.

Systematic experimental and theoretical investigations of absorptive dissymmetry factor across the helical fluorenone series (*M*-**A1** to *M*-**A20**) revealed significant substituent-dependent modulation of chiroptical properties. Notably, positional isomerism markedly influenced the $|g_{abs}|$. The installation of methyl group from the 2- to 6-position (*M*-**A2** → *M*-**A6**) reduced $|g_{abs}|$ value from $8.3 \times 10^{-3}$ to $5.2 \times 10^{-3}$ (Fig. 6E, black labels). Next, by fixing the substituents at 4,4'-positions, it revealed that the steric effects substantially impacted chiroptical responses. Increasing the bulk of substituent from hydrogen (*M*-**A1**, $|g_{abs}| = 7.7 \times 10^{-3}$) to phenyl (*M*-**A15**, $|g_{abs}| = 1.1 \times 10^{-2}$) produced progressive enhancement of dissymmetry factors (Fig. 6F). In these examples, the theoretical $g_{cal}$ and $g_{abs}$ factors exhibited consistent trends with variations in peripheral substituents (Fig. 6E, F, red labels). In addition, enhanced conjugation substitutions significantly improved chiroptical performance, such as 3-phenyl substituted *M*-**A15** and [9]-helical fluorenone **A20** ($g_{abs}$ as $9.9 \times 10^{-3}$ at 366 nm). This comprehensive study shows that strategic modification of peripheral substituents on helical fluorenones enables precise tuning of chiroptical response magnitude through synergistic control of electronic environment and steric demands. Furthermore, the circularly polarized luminescence (CPL) spectra of some products were tested (for details see Supplementary Information Figs. S103–S109). A mirror-image relationship was observed in of (*P, S*)-**C1** and (*M, R*)-**C1** in dichloromethane, with a luminescence dissymmetry factor $|g_{lum}|$ of $3.6 \times 10^{-4}$ at 500 nm. (*P, R*)-**C1** and (*M, S*)-**C1** also exhibited mirror-imaged CPL spectra, in which the CPL emission band was red-shifted to approximately 505 nm, and the $|g_{lum}|$ value was determined to be $3.8 \times 10^{-4}$. The inversion of stereocenters scarcely altered the CPL behavior, indicating that the results are primarily governed by the direction of the helical skeleton. Compound (*P, S*)-**C19** exhibited the strongest CPL emission among the series, with its luminescence dissymmetry factor $|g_{lum}|$ measured at $1.1 \times 10^{-3}$ at 560 nm. The helicenone substrate *M*-**A10** displayed CPL in DCM solution at 540 nm with a $|g_{lum}|$ value of $1.2 \times 10^{-3}$. These CD and CPL results clearly demonstrate that optically enriched [7]helical fluorenones and ring-expanded [7]helical phenanthrenones maintain their chirality in both the ground and excited states.

## Discussion

In summary, we have achieved an enantioselective homologation of racemic helical fluorenones catalyzed by a scandium complex with a meticulously designed *N,N'*-dioxide ligand under mild reaction condition. This process provided access to a series of ring-expanded helical phenanthrenones with helical and central chiral elements in high diastereo- and enantioselectivity, meanwhile less reactive helical fluorenone enantiomers were efficiently recovered with high optical activity under kinetic resolution. For unsymmetric helical fluorenones, the aryl migration during the homologative ring expansion process also demonstrated interesting regioselectivity. Specifically, with *P*-helical fluorenones, the smaller aryl group preferentially migrates, whereas the opposite preference was observed conversely. Further transformation of helical fluorenone gave rise to several functionalized helical compounds. Moreover, the photophysical chiroptical

https://doi.org/10.1038/s41467-025-64151-1

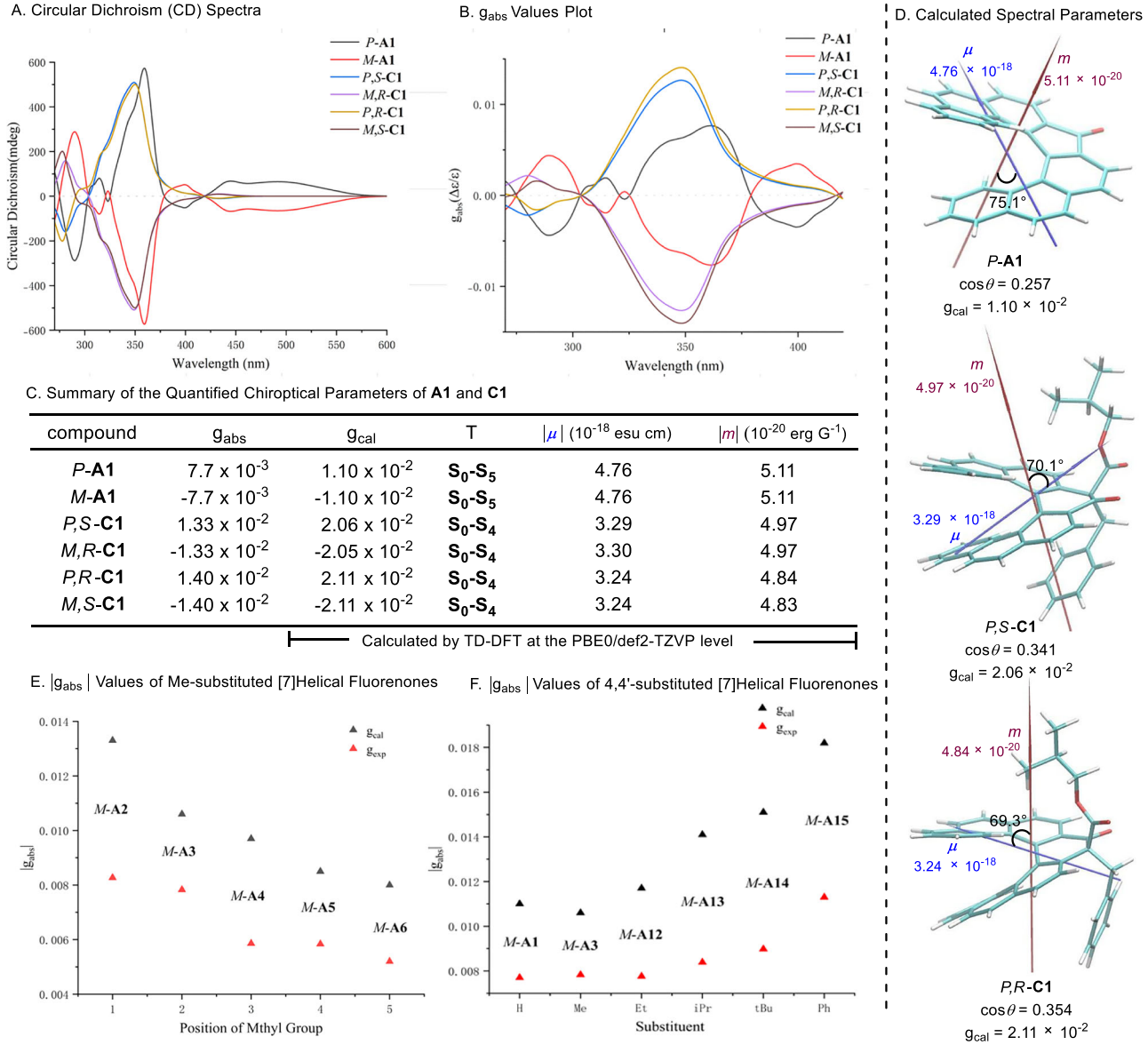


| compound | $g_{abs}$ | $g_{cal}$ | T | $\|\mu\|$ ($10^{-18}$ esu cm) | $\|m\|$ ($10^{-20}$ erg $G^{-1}$) |
|---|---|---|---|---|---|
| *P*-**A1** | 7.7 x $10^{-3}$ | 1.10 x $10^{-2}$ | $S_0$-$S_5$ | 4.76 | 5.11 |
| *M*-**A1** | -7.7 x $10^{-3}$ | -1.10 x $10^{-2}$ | $S_0$-$S_5$ | 4.76 | 5.11 |
| *P,S*-**C1** | 1.33 x $10^{-2}$ | 2.06 x $10^{-2}$ | $S_0$-$S_4$ | 3.29 | 4.97 |
| *M,R*-**C1** | -1.33 x $10^{-2}$ | -2.05 x $10^{-2}$ | $S_0$-$S_4$ | 3.30 | 4.97 |
| *P,R*-**C1** | 1.40 x $10^{-2}$ | 2.11 x $10^{-2}$ | $S_0$-$S_4$ | 3.24 | 4.84 |
| *M,S*-**C1** | -1.40 x $10^{-2}$ | -2.11 x $10^{-2}$ | $S_0$-$S_4$ | 3.24 | 4.83 |

**Fig. 6 | Photophysical chiroptical properties studies. A** Circular dichroism (CD) spectra of **A1** and **C1**. **B** $g_{abs}$ values plot of **A1** and **C1**. **C**, **D**) TD-DFT calculated parameters of **A1** and **C1** at the PBE0/def2-TZVP theory level. **μ**: transition electric dipole moments. **m**: transition magnetic dipole moments. **θ**: angle between **m** and **μ**. **E**, **F** Comparison between theoretical ($g_{cal}$) and experimental ($g_{exp}$) dissymmetry factors.

properties of these helical compounds were systematically investigated, specifically examining the regulatory effects of substituents on the electronic circular dichroism of these helical compounds. Through synergistic integration of theoretical calculations and experimental data, we elucidated the mechanism underlying the enhanced electronic circular dichroism response in penanthrenones enabled by homologation-driven skeletal editing. This methodology not only provides an efficient approach for synthesizing optically pure helical fluorenones and helical phenanthrenones but also offers extensive experimental and theoretical insights for designing molecular architectures with enhanced electronic circular dichroism responses. Further application of the catalysts system for other transformations and explore the usage of these helical compounds are undergoing.

## Methods

### General procedure for the kinetic resolution of helical fluorenones

To a dry test tube under nitrogen atmosphere were added $Sc(OTf)_3$ (3.2 mg, 0.0065 mmol, 13 mol%), ligand **NO-3** (5.4 mg, 0.005 mmol, 10 mol%) in THF (1.0 mL), and the mixture was stirred at 35 °C for 20 min. Substrate **A** (19 mg, 0.05 mmol, 1.0 equiv.) was added to the test tube after THF was evaporated. Then the resulting mixture was stirred at 35 °C for 20 min, after cooling to 0 °C substrate **B** (18 μL, 0.0625 mmol, 1.5 equiv.) was added. The reaction solution was stirred under such conditions. After the ee value of spiral fluorenone **A** was increased to more than 90% (detected by chiral HPLC), the reaction solution was filtered by a short silica gel column to quench the reaction, and the solution was concentrated under reduced pressure. The crude residue was subjected to column chromatography on silica gel (2:1 v/v Pet:DCM as the eluent) to afford the product (*P*, *S*)-**C** and *M*-**A**.

## Data availability

Crystallographic data for the structures reported in this study have been deposited at the Cambridge Crystallographic Data Centre, under deposition numbers CCDC 2423529 [for major diastereomer of *rac*-**C6**], 2423528 [for (*M*)-**A18**], CCDC 2472266 [for (*M, S*)-**C24'**], and CCDC 2475114 [for major diastereomer of *rac*-**C25**]. Copies of the data can be obtained free of charge at https://www.ccdc.cam.ac.uk/structures/.

The data supporting the findings of this work are provided in the Supplementary Information, including experimental procedures and characterization of new compounds. All data are available from the corresponding author upon request. Source Data are provided with this manuscript. Source data are provided with this paper.

## References


1. Gingras, M. One hundred years of helicene chemistry. Part 1: non-stereoselective syntheses of carbohelicenes. *Chem. Soc. Rev.* **42**, 968–1006 (2013).
2. Nakai, Y., Mori, T. & Inoue, Y. Theoretical and experimental studies on circular dichroism of Carbo[n]helicenes. *J. Phys. Chem. A.* **116**, 7372–7385 (2012).
3. Mori, T. Chiroptical properties of symmetric double, triple, and multiple helicenes. *Chem. Rev.* **121**, 2373–2412 (2021).
4. Nowak-Król, A., Geppert, P. T. & Naveen, K. R. Boron-containing helicenes as new generation of chiral materials: opportunities and challenges of leaving the flatland. *Chem. Sci.* **15**, 7408–7440 (2024).
5. Maeda, C. & Ema, T. Recent development of Azahelicenes showing circularly polarized luminescence. *Chem. Commun.* **61**, 4757–4773 (2025).
6. Gingras, M. One hundred years of helicene chemistry. Part 3: applications and properties of carbohelicenes. *Chem. Soc. Rev.* **42**, 1051–1095 (2013).
7. Brandt, J. R., Salerno, F. & Fuchter, M. J. The added value of small-molecule chirality in technological applications. *Nat. Rev. Chem.* **1**, 45–56 (2017).
8. Kelly, T. R. et al. Progress toward a rationally designed, chemically powered rotary molecular motor. *J. Am. Chem. Soc.* **129**, 376–386 (2007).
9. Takenaka, N., Sarangthem, R. S. & Captain, B. Helical chiral pyridine *N*-Oxides: a new family of asymmetric catalysts. *Angew. Chem. Int. Ed.* **47**, 9708–9710 (2008).
10. Shcherbina, M. A. et al. Hollow six-stranded helical columns of a helicene. *Angew. Chem. Int. Ed.* **48**, 7837–7840 (2009).
11. Yavari, K. et al. Helicenes with embedded phosphole units in enantioselective gold catalysis. *Angew. Chem. Int. Ed.* **53**, 861–865 (2014).
12. Gingras, M. One hundred years of helicene chemistry. Part 2: stereoselective syntheses and chiral separations of carbohelicenes. *Chem. Soc. Rev.* **42**, 1007–1050 (2013).
13. Tanaka, K., Kimura, Y. & Murayama, K. Enantioselective helicene synthesis by rhodium-catalyzed [2+2+2] cycloadditions. *Bull. Chem. Soc. Jpn.* **88**, 375–385 (2015).
14. Dhbaibi, K., Favereau, L. & Crassous, J. Enantioenriched helicenes and helicenoids containing main-group elements (B, Si, N, P). *Chem. Rev.* **119**, 8846–8953 (2019).
15. Stara, I. G. & Stary, I. Helically chiral aromatics: the synthesis of helicenes by [2+2+2] cycloisomerization of π-electron system. *Acc. Chem. Res.* **53**, 144–158 (2020).
16. Wang, Y., Wu, Z. G. & Shi, F. Advances in catalytic enantioselective synthesis of chiral helicenes and helicenoids. *Chem. Catal.* **2**, 3077–3111 (2022).
17. Fan, P., Li, L. & Qian, D. Catalytic asymmetric construction of helicenes via transformation of biaryls. *Org. Biomol. Chem.* **22**, 3186–3197 (2024).
18. Yang, H., Feng, H. & Zhou, L. Asymmetric synthesis of helicenes from centrally chiral precursors. *Eur. J. Org. Chem.* **27**, e202400671 (2024).
19. Huang, Q., Tang, Y., Zhang, C., Wang, Z. & Dai, L. Enantioselective synthesis of helically chiral molecules enabled by asymmetric organocatalysis. *ACS Catal.* **14**, 16256–16265 (2024).
20. Liu, W., Qin, T. R., Xie, W. S. & Yang, X. Y. Catalytic enantioselective synthesis of helicenes. *Chem. Eur. J.* **28**, e202202369 (2022).
21. Kötzner, L., Webber, M. J., Martínez, A., Fusco, C. D. & List, B. Asymmetric catalysis on the nanoscale: the organocatalytic approach to helicenes. *Angew. Chem. Int. Ed.* **53**, 5202–5205 (2014).
22. Sako, M. et al. Efficient enantioselective synthesis of oxahelicenes using redox/acid cooperative catalysts. *J. Am. Chem. Soc.* **138**, 11481–11484 (2016).
23. Oyama, H. et al. Synthesis and properties of [7]Helicene-like compounds fused with a fluorene unit. *Org. Lett.* **18**, 3654–3657 (2016).
24. González-Fernández, E. et al. Enantioselective synthesis of [6]Carbohelicenes. *J. Am. Chem. Soc.* **139**, 1428–1431 (2017).
25. Nicholls, L. D. M. et al. TADDOL-derived cationic phosphonites: toward an effective enantioselective synthesis of [6]Helicenes via Au-catalyzed alkyne hydroarylation. *ACS Catal.* **8**, 6079–6085 (2018).
26. Jia, S., Li, S., Liu, Y., Qin, W. & Yan, H. Enantioselective control of both helical and axial stereogenic elements though an organocatalytic approach. *Angew. Chem. Int. Ed.* **58**, 18496–18501 (2019).
27. Liu, P., Bao, X., Naubron, J. V., Chentouf, S. & Humbel, S. Simultaneous control of central and helical chiralities: expedient helicoselective synthesis of Dioxa[6]helicenes. *J. Am. Chem. Soc.* **142**, 16199–16204 (2020).
28. Yubuta, A. et al. Enantioselective synthesis of triple helicenes by cross cyclotrimerization of a helicenyl aryne and alkynes via dynamic kinetic resolution. *J. Am. Chem. Soc.* **142**, 10025–10033 (2020).
29. Kinoshita, S., Yamano, R., Shibata, Y., Tanaka, Y. & Tanaka, K. Rhodium-catalyzed highly diastereo- and enantioselective synthesis of a configurationally stable S-shaped double helicene-like molecule. *Angew. Chem. Int. Ed.* **59**, 11020–11027 (2020).
30. Wang, Q., Zhang, W., Zheng, C., Gu, Q. & You, S. Enantioselective synthesis of azoniahelicenes by Rh-catalyzed C–H annulation with alkynes. *J. Am. Chem. Soc.* **143**, 114–120 (2021).
31. Feng, J. et al. Ring-expansion strategy for α-Aryl azahelicene construction: building blocks for optoelectronic materials. *Org. Lett.* **23**, 8056–8061 (2021).
32. Wu, J. et al. Organocatalytic dynamic kinetic resolution enabled asymmetric synthesis of phosphorus-containing chiral helicenes. *Angew. Chem. Int. Ed.* **62**, e202309515 (2023).
33. Liu, W. et al. Enantioselective synthesis of azahelicenes through organocatalyzed multicomponent reactions. *Angew. Chem. Int. Ed.* **62**, e202303430 (2023).
34. Li, C. W. et al. Enantioselective Synthesis of chiral quinohelicenes through sequential organocatalyzed povarov reaction and oxidative aromatization. *Nat. Commun.* **14**, 3380–3389 (2023).
35. Wang, L. M., Duan, L. H., Hong, B. Q. & Gu, Z. H. Divergent synthesis of helical ketone enabled by rearrangement of spiro carbocation. *Org. Lett.* **25**, 1912–1917 (2023).
36. Morita, F. et al. A design and enantioselective synthesis of 3d π-extended carbohelicenes for circularly polarized luminescence. *Nat. Synth.* **3**, 774–786 (2024).
37. Xu, W., Zhang, R., Wang, H., Chen, J. & Zhou, L. Helicoselective synthesis of indolohelicenoids through organocatalytic central-to-helical chirality conversion. *Angew. Chem. Int. Ed.* **63**, e202318021 (2024).
38. Fu, W. et al. Enantioselective synthesis, (Chir)optical properties, and postsynthetic functionalization of furan-containing Oxa[5]-, Oxa[6]-, and Dioxa[6]helicenes. *CCS Chem.* **6**, 2439–2451 (2024).
39. Qin, T. R., Xie, W. S., Liu, W. & Yang, X. Y. Diverse enantioselective synthesis of Hetero[7]helicenes via an organocatalyzed double annulation strategy. *Org. Chem. Front.* **12**, 1417–1424 (2025).
40. Tanaka, K., Fukawa, N., Suda, T. & Keiichi, N. One-step construction of five successive rings by rhodium catalyzed intermolecular double [2+2+2] cycloaddition: enantioenriched [9]Helicene-like molecules. *Angew. Chem. Int. Ed.* **48**, 5470–5473 (2009).

41. Sawada, Y. et al. Rhodium-catalyzed enantioselective synthesis, crystal structures, and photophysical properties of helically chiral 1,1′-bitriphenylenes. *J. Am. Chem. Soc.* **134**, 4080–4083 (2012).
42. Gross, B. M. & Oestreich, M. The trityl cation embedded into a [7] Helicene-like backbone: preparation and application as a lewis acid catalyst. *Synthesis* **53**, 2512–2516 (2021).
43. Dong, S. X., Liu, X. H. & Feng, X. M. Asymmetric catalytic rearrangements with α-Diazocarbonyl compounds. *Acc. Chem. Res.* **55**, 415–428 (2022).
44. Chen, D.-F., Gong, L.-Z. & Feng Chiral, N. *N′*-Dioxide ligands: uniqueness and impacts. *Org. Chem. Front.* **10**, 3676–3683 (2023).
45. Li, W. et al. Catalytic asymmetric roskamp reaction of α-Alkyl-α-diazoesters with aromatic aldehydes: highly enantioselective synthesis of α-Alkyl-β-keto Esters. *J. Am. Chem. Soc.* **132**, 8532–8533 (2010).
46. Li, W. et al. A catalytic asymmetric ring-expansion reaction of isatins and α-Alkyl-α-diazoesters: highly efficient synthesis of functionalized 2-quinolone derivatives. *Angew. Chem. Int. Ed.* **51**, 8644–8647 (2012).
47. Tan, F. et al. Catalytic ASYMMETRIC HOMOLOGATION OF KETONEs with α-Alkyl α-Diazo Esters. *J. Am. Chem. Soc.* **143**, 2394–2402 (2021).
48. Hu, K., Q.Zhang, D., Wang, S. Y., Lin, L. & Feng, X. M. Catalytic asymmetric [4+1] cycloaddition to synthesize chiral pyrazoline-spirooxindoles. *Org. Chem. Front.* **10**, 2422–2428 (2023).
49. Li, S. Y. et al. Enantioselective photochemical carbene insertion into C–C and C–H Bonds of 1,3-diketones by a guanidine-amide organocatalyst. *ACS Catal.* **13**, 4656–4666 (2023).
50. Liu, Z. Z. et al. Iron-catalyzed asymmetric imidation of sulfides via sterically biased nitrene transfer. *J. Am. Chem. Soc.* **146**, 18050–18060 (2024).
51. He, X. et al. Asymmetric carbene insertion into Se-S bonds by synergistic Rh(II)/guanidine catalysis involving chalcogen-bond assistance. *Angew. Chem. Int. Ed.* **64**, e202417636 (2025).
52. Xiao, Z. J. et al. Asymmetric catalytic synthesis of allylic sulfenamides from vinyl α-Diazo compounds by a rearrangement route. *Angew. Chem. Int. Ed.* **64**, e202414712 (2025).
53. Yang, Z. D. et al. Metal-controlled enantiodivergent tandem rearrangement to synthesize 2H-Azirines. *Angew. Chem. Int. Ed.* **64**, e202505725 (2025).
54. Cao, W. D., Liu, X. H. & Feng, X. M. Asymmetric catalytic radical reactions enabled by chiral *N*, *N′*-dioxide–metal complexes. *Acc. Chem. Res.* **58**, 2496–2510 (2025).
55. Dong, S. X., Cao, W. D., Pu, M. P., Liu, X. H. & Feng, X. M. Ligand Acceleration in chiral lewis acid catalysis. *CCS Chem.* **5**, 2717–2735 (2023).
56. Humphrey, W., Dalke, A. & Schulten, K. VMD: visual molecular dynamics. *J. Comput. Chem.* **14**, 33–38 (1996).
57. Lu, T. & Chen, F. Multiwfn: a multifunctional wavefunction analyzer. *J. Comput. Chem.* **33**, 580–592 (2012).
58. Liu, Z., Lu, T. & Chen, Q. An sp-hybridized all-carboatomic ring, Cyclo[18]carbon: electronic structure, electronic spectrum, and optical nonlinearity. *Carbon* **165**, 461–467 (2020).
59. Li, J. et al. B, N-embedded double hetero[7]helicenes with strong chiroptical responses in the visible light region. *J. Am. Chem. Soc.* **143**, 17958–17963 (2021).

## Acknowledgements

We appreciate the financial support of the National Natural Science Foundation of China (22188101), and Sichuan University (2020SCUNL204). We are grateful to Prof. Minghua Liu and Ms. Xin Wen from Institute of Chemistry Chinese Academy of Sciences for assistance with CPL analysis.

## Author contributions

L.S.Y. preformed the experiments and the DFT calculation. Y. S. preformed some of the substrates. F.L.W. and L.Z.Z. assisted with discussions of experimental data. Z.Y. repeated the data. Z.Y.Q. preformed X-ray analysis. F.X.M., F.L.W., and L.X.H. prepared this manuscript and the supplementary information.

## Competing interests

The authors declare no competing interests.

## Additional information

**Supplementary information** The online version contains supplementary material available at https://doi.org/10.1038/s41467-025-64151-1.

**Correspondence** and requests for materials should be addressed to Liang-Wen Feng or Xiaohua Liu.

**Peer review information** *Nature Communications* thanks Xiaoyu Yang and the other anonymous reviewer(s) for their contribution to the peer review of this work. A peer review file is available.